The effect of head-tracking resolution on the stability and performance of a local active noise control headrest system

Chung Kwan Lai, Jordan Cheer, and Chuang Shi

Institute of Sound and Vibration Research, University of Southampton,

Southampton SO17 1BJ, United Kingdom^a

Incorporating head-tracking techniques into local active noise control headrest systems enables the plant model used in the controller to be updated dynamically as the user moves their head. This reduces the mismatch between the plant model and the physical plant responses from the secondary sources to the users' ears, which increases the achievable noise reduction when head movement occurs. In practice, since the plant models for different head positions must be identified during a calibration procedure, it is necessary to limit the head-tracking resolution to constrain the complexity of this procedure. This leads to errors between the physical and modelled plant responses as the user's head moves, which impacts the control system's stability and performance. However, the relationship between the control system behaviour and the tracking accuracy is not well understood. This paper investigates the impact of head-tracking resolution, considering translational and rotational movements, on the stability and performance of an active headrest. Assuming the error signals at the user's ears are available for adaptive control, it is shown that the system has an upper-frequency limit beyond which controller instability occurs, and this frequency is influenced by the tracking resolution, the initial head position, and the type of head movement.

10

11

12

13

14

15

16

17

^aJ.Cheer@soton.ac.uk

18 I. INTRODUCTION

Active noise control techniques have gained significant interest in a variety of applica-19 tions for their ability to reduce unwanted disturbances using secondary sound sources. ^{1,2} A variety of different strategies have been proposed to realise active noise control, however, considering the spatial extent of the achieved control, they can be broadly categorised into global and local strategies. Global control aims to attenuate the unwanted sound throughout the entire acoustic space, which is typically an enclosure, whilst local control aims to achieve attenuation in a targeted region, which allows control to be achieved up to higher 25 frequencies. One practical realisation of local noise control is the active headrest, which incorporates secondary loudspeakers into a headrest and achieves local control at the ears of a seated listener.³⁻⁵ In general, local control is limited by the size of the zones of quiet, which are generated around the error sensors. For example, the size of the 10 dB zone of quiet, defined as the region within which sound attenuation of at least 10 dB is achieved, is of the order of 1/10-th of the acoustic wavelength in a diffuse sound field. This means that 31 as frequency increases the zone of quiet decreases in size. In practice, because the physical error sensors cannot be placed too close to the listener's ears due to safety and potential user discomfort, the finite size of the zone of quiet limits the bandwidth of local active control.

Although virtual sensing techniques can help to extend the upper-frequency limit of control, the performance in headrest applications is still degraded by listener head movement because the zone of quiet is fixed in space. To overcome this limitation, head tracking technology can be used to detect the current position of the head, and correspondingly update the controller.⁷⁻⁹ In particular, head movements result in a change in the response between the secondary loudspeakers and the error microphones and this plant response change must be reflected in a change in the plant model used in the controller. This generally relies on the utilisation of a set of pre-determined plant models that correspond to the plant responses measured with the head located at a finite grid of head positions within the vicinity of the headrest during a calibration phase. As a result, the predetermined values that correspond to the position closest to the current head coordinate are generally utilised, in a nearest neighbour-type approach. This helps to reduce the mismatch between the plant model used by the control system and the physical plant response, and therefore allows the zone of quiet to be dynamically repositioned to the ear location as the head moves. This has been shown in previous work to be able to achieve significant attenuation at the listener's ears at frequencies up to at least 1 kHz.8 However, this previous work did not consider the effect of a mismatch between the physical position of the head and the assumed position of the head and thus differences between the physical and modelled plant responses. To minimise these errors, the plant responses would ideally be measured during the calibration phase over an extremely fine grid so that, assuming that the headtracker is able to exactly identify the head position, the difference between the nearest available grid position and the physical head position would be small. This would in turn mean that the difference between the pre-determined plant response and the physical plant response would also be small. However, this would require a lengthy calibration process to measure the plant response for many head positions and orientations. As a result, it is necessary to reach a trade-off between the complexity of the calibration procedure and the resulting accuracy of the plant models available to the controller during operation. In addition, in practice it may also
be necessary to consider the accuracy with which the headtracker is able to determine the
position and orientation of the listener's head, since this may lead to a further mismatch
between the modelled and physical plant responses; although modern head-tracking systems
have high levels of accuracy¹⁰, which will generally exceed the resolution of a practicable
calibration grid.

To help overcome this limitation, and improve the robustness of active headrest systems 67 to head movement, various modifications to their design have been proposed. For example, in previous studies^{11,12} a method is proposed to determine a plant model through various optimisation methods that help to ensure robustness to slight head movements. Likewise, some research effort has focused on enlarging the zone of quiet by repositioning the location 71 of the error microphones and introducing additional secondary loudspeakers to minimise the acoustic velocity in a direction perpendicular to the surface of the head. 13,14 Alternatively, the plant model at head positions not included in the calibration phase could be estimated via higher-order interpolation between the available plant models.¹⁵ While there has been previous work conducted to investigate the significance of performance degradation under head movements^{8,16–18}, this work primarily presents a comparison between scenarios with 77 and without head-tracking. This paper will present an experimental investigation into the effect of the calibration grid resolution on control stability and performance for translational and rotational head movements, across the region in which the user's head may be located, in a tonal local active noise control headrest. In this work it is assumed that the error signals at the ears are known and used for control, which reflects previous work in the area^{19,20}, but

also focuses the provided system design insight on the effect of changes in the plant response rather than on the performance of virtual sensing techniques.²¹ Additionally, in order to provide a contribution that focuses on the fundamental limitations imposed by head movements alone, without restricting the findings to a particular final application, the underlying room dynamics are not considered here. This approach helps to bridge the research gap for future work where the room acoustic response is considered and allows a distinction to be made between the limitations due to head movement alone and those due to the acoustical response of the room. Consequently, the work presented in this paper is able to demonstrate how the control stability and performance of the headtracking-equipped active headrest sys-91 tem can be influenced by the head-tracking resolution, initial head position, and the type of head movement. The paper is structured as follows: Section II describes the physical arrangement of the assumed active headrest system and the control strategy; Section III explores the effect of both translational and rotational head movements on the plant responses; Section IV presents an investigation into the effect of head tracking resolution on the control stability and performance and Section V draws conclusions.

98 II. HEADTRACKER-EQUIPPED MULTICHANNEL FEEDFORWARD ACTIVE

99 NOISE CONTROL SYSTEM

To motivate the following investigation, this section will first describe the physical arrangement of the headtracker-equipped active headrest system, before describing the feedforward control strategy that will be utilised in the following studies.

A. Physical setup of the headtracker-equipped active headrest

103

Figure 1 shows the experimental arrangement of the active headrest in an anechoic cham-104 ber. The measurements have been conducted in an anechoic chamber to ensure that changes 105 in the plant responses are due to head movement alone, rather than any interactions with the 106 acoustic response of the room. This allows the work to focus on the fundamental limitations 107 imposed by head movements without restricting the findings to a particular final application. 108 The two secondary loudspeakers, denoted as L1 and L2, are used to attenuate the pressures 100 at the locations of the error microphones, denoted E1 and E2, which are located at the ears of the dummy head. The primary disturbance is generated by a single loudspeaker 111 located directly in front of the headrest system at a distance of 3 m. The dummy head is 112 positioned and rotated using a robotic positioning system to ensure precise alignment with the intended coordinate and repeatability, so that a reliable analysis of the effects of head 114 movement can be conducted with respect to the head position and orientation. A series of 115 measurements, which utilise an exponential sine sweep to remove any potential non-linear 116 behaviour introduced by the loudspeaker's characteristics²², have been conducted to obtain 117 the secondary plant responses and the disturbance signals for each head position within a 118 discrete translational grid of $(0.4 \text{ m} \times 0.2 \text{ m})$, with a resolution of 2.5 cm, and a discrete 119 rotational grid ranging from -27° to $+27^{\circ}$, with a resolution of 9° , as illustrated in Figure 2. 120 The translational grid resolution used here is twice that used in previous work⁸, where the 121 use of head-tracking was shown to enable active control to be achieved up to around 1 kHz 122 in a headrest system. The increased resolution utilised here allows an exploration into the

effect of differences between the physical and the modelled head position; for example, the responses measured across the 2.5 cm grid can be used to represent the physical head po-125 sition responses, while assessing the modelling accuracy for the 5 cm grid resolution used in previous work. Similar logic has been utilised in the selection of the angular resolution, 127 where previous work has used an angular resolution of 15°. 23 Although a finer resolution 128 would allow an investigation into the effect of head-tracking to be conducted up to higher 129 frequencies, the selected translational and angular resolution gives a total of 153 translation 130 grid measurement points, with seven angular measurements at each point, which leads to a 131 total of 1071 head position and orientation measurements. Increasing the translational grid 132 resolution by a factor of two to 1.25 cm would increase the number of required measurements 133 to almost 4000, which would be rather impractical. Translational movement in the sway 134 (left-right) and surge (front-back) directions has been investigated here, whilst movement in 135 the heave (up-down) direction has been left for future work. Similarly, rotational movement 136 in the yaw direction has been explored, whilst both pitch and roll head rotations have been 137 left for future work. The rationale for exploring the sway, surge and yaw degrees of freedom 138 in this work is to constrain the considered problem and focus on the head movements that are likely to be more significant and frequently encountered in an active headrest system; 140 that said, exploration of the other degrees of freedom may become more relevant in certain 141 applications and so should be explored in future work.

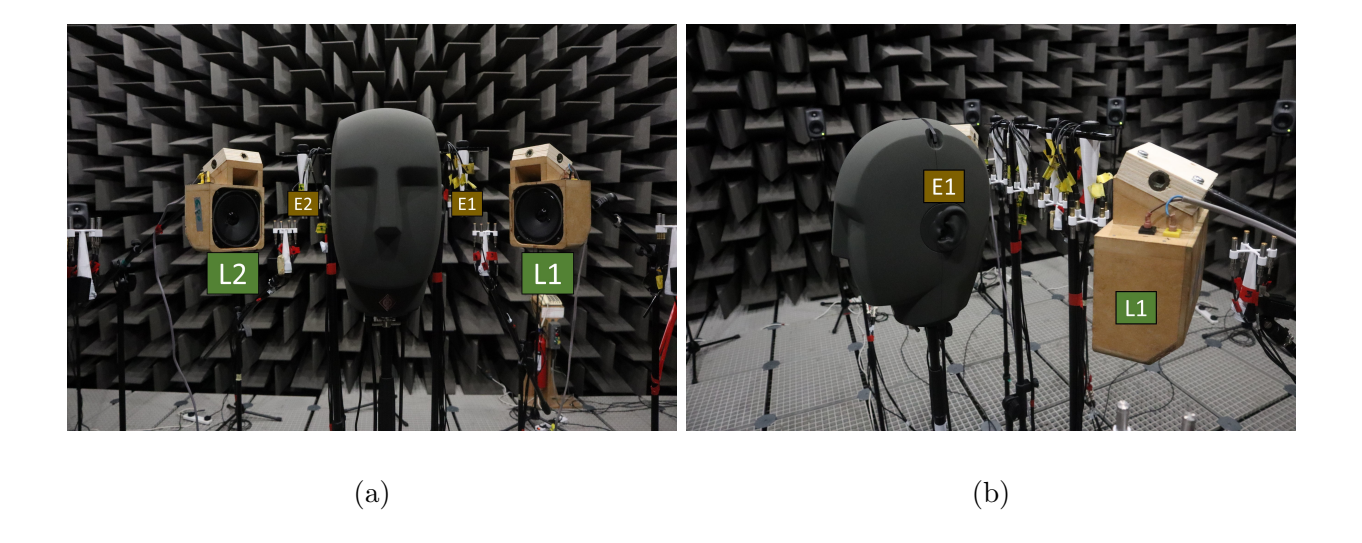


FIG. 1: The arrangement of the secondary loudspeakers, L1 and L2, in the active headrest placed in the anechoic chamber, together with the error microphones in the ears of the dummy head, E1 and E2. The front and side views are shown in (a) and (b) respectively.

B. Multichannel feedforward active control strategy

143

Active noise control headrests have been realised using both feedforward and feedback 144 control strategies. 24 In general, feedforward control strategies are utilised in cases where a 145 time-advanced and coherent reference signal is available to the controller. This generally applies in cases where control of noise generated by rotational machinery is considered, 147 which is perhaps the most relevant application for the tonal noise control problem assumed 148 in this paper. Therefore, a tonal feedforward control strategy has been utilised where it is assumed that a perfect reference signal is available and the system is linear. In practice, 150 the assumption that the plant response is linear will be dependent on the specifics of the 151 system realisation, particularly including the loudspeaker which may operate in a non-linear 152 regime depending on its power handling capability and the amplitude of the disturbance

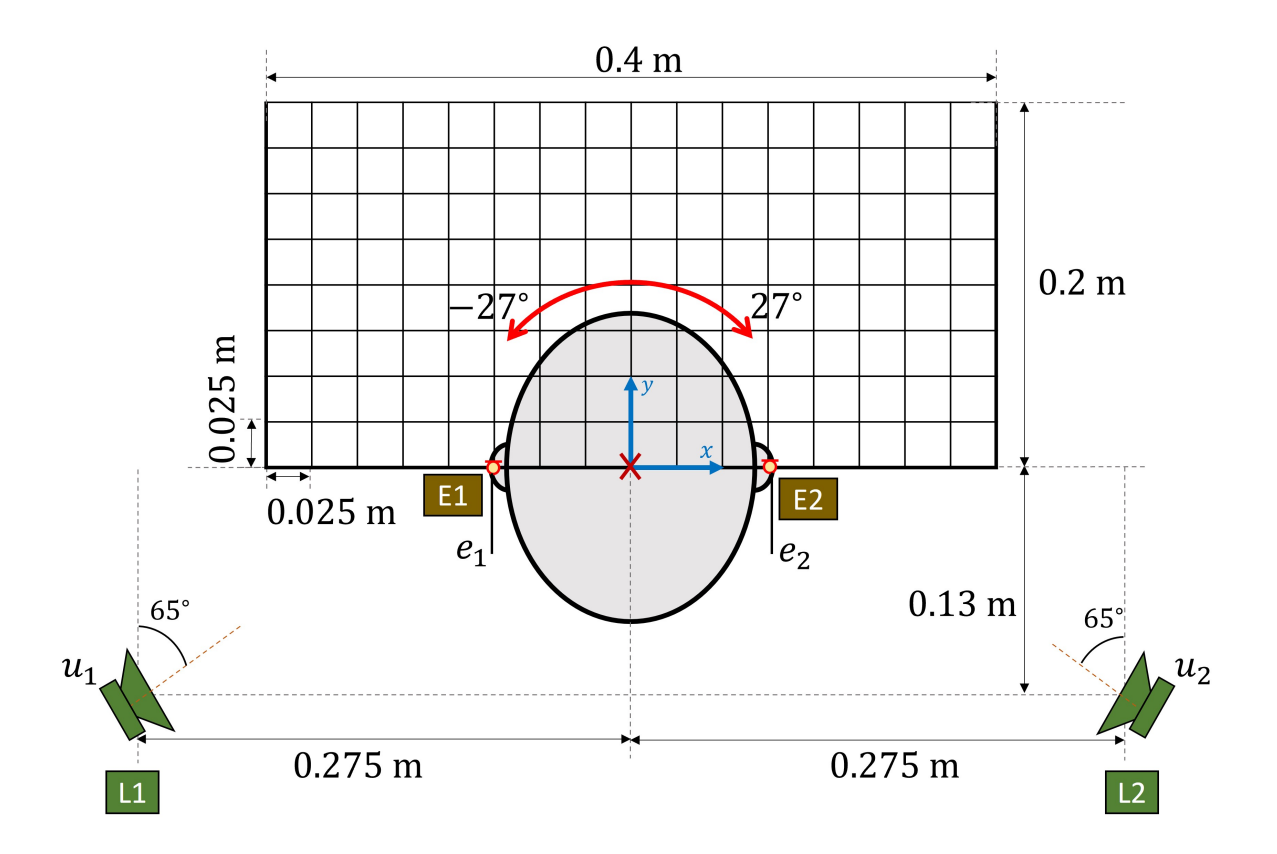


FIG. 2: The geometry for the active headrest system. The head translates in the sway (left/right) and surge (front/back) translational directions over an area of (0.4 m \times 0.2 m), and rotates within a yaw range of -27° to $+27^{\circ}$. The minimum grid spacing for the translational and rotational grid were defined as 0.025 m and 9° respectively.

pressures being controlled. Although a variety of control strategies have been developed for the control of non-linear systems²⁵, it is quite typical to assume linear behaviour since this can often be ensured by appropriate specification of the control loudspeakers. The assumption that a perfect reference signal is available mean that the results presented here are only fully representative of a tonal control problem. When the disturbance noise is stochastic in nature and generated by multiple uncorrelated sources there is a need to utilise multiple reference signals that are both coherent and time-advanced with respect to the error signals. This situation occurs, for example, when attempting to control road noise in a vehicle cabin and it is then realistic for the available reference signals to be imperfect and this will inherently limit the maximum level of achievable control. That said, the linearity and perfect reference signal assumptions have been widely assumed in the active control literature², since exploring system limitations within these assumptions can provide clear insight into the physical limitations of the controller.

Figure 3 shows the multichannel feedforward control block diagram, which assumes that
the error signals, **e** at the ears are perfectly known so that they are used directly to adapt
the control filters, **W**. Assuming that the disturbance to be controlled is tonal, then the
cost function to be minimised by the control system shown in Figure 3 can be defined in the
frequency domain as the sum of the squared error signals given by

$$J = \mathbb{E}\left[\mathbf{e}^{\mathrm{H}}\mathbf{e} + \beta\mathbf{u}^{\mathrm{H}}\mathbf{u}\right] \tag{1}$$

where $\mathbf{e} = [e_1 \quad e_2]^{\mathrm{T}}$ denotes a complex vector of the two error signals measured at the ears, $\mathbf{u} = [u_1 \quad u_2]^{\mathrm{T}}$ denotes the vector of control signals used to drive the two headrest loudspeakers, and β denotes the regularisation, or leakage parameter. From Figure 3 it can be seen that the vector of error signals can be expressed as

$$\mathbf{e} = \mathbf{d} + \mathbf{G}\mathbf{u} \tag{2}$$

where $\mathbf{d} = [d_1 \quad d_2]^{\mathrm{T}}$ denotes the vector of disturbance signals measured by the error microphones at the ears, and \mathbf{G} denotes the physical plant responses between the headrest loudspeakers and the error microphones. Under ideal conditions, where the disturbance signals and the plant responses are perfectly known and are steady-state, the vector of optimum control signals can be calculated by substituting Equation (2) into Equation (1), followed by differentiating with respect to the real and imaginary parts of **u** to give

$$\mathbf{u}_{opt} = -\left[\mathbf{G}^{\mathrm{H}}\mathbf{G} + \beta \mathbf{I}\right]^{-1}\mathbf{G}^{\mathrm{H}}\mathbf{d}.$$
 (3)

In practice, however, the plant response may only be known with some level of uncertainty,
due for example to head movements and associated modelling errors, and the disturbance
may also vary over time, leading to the need for the implementation of an adaptive controller.

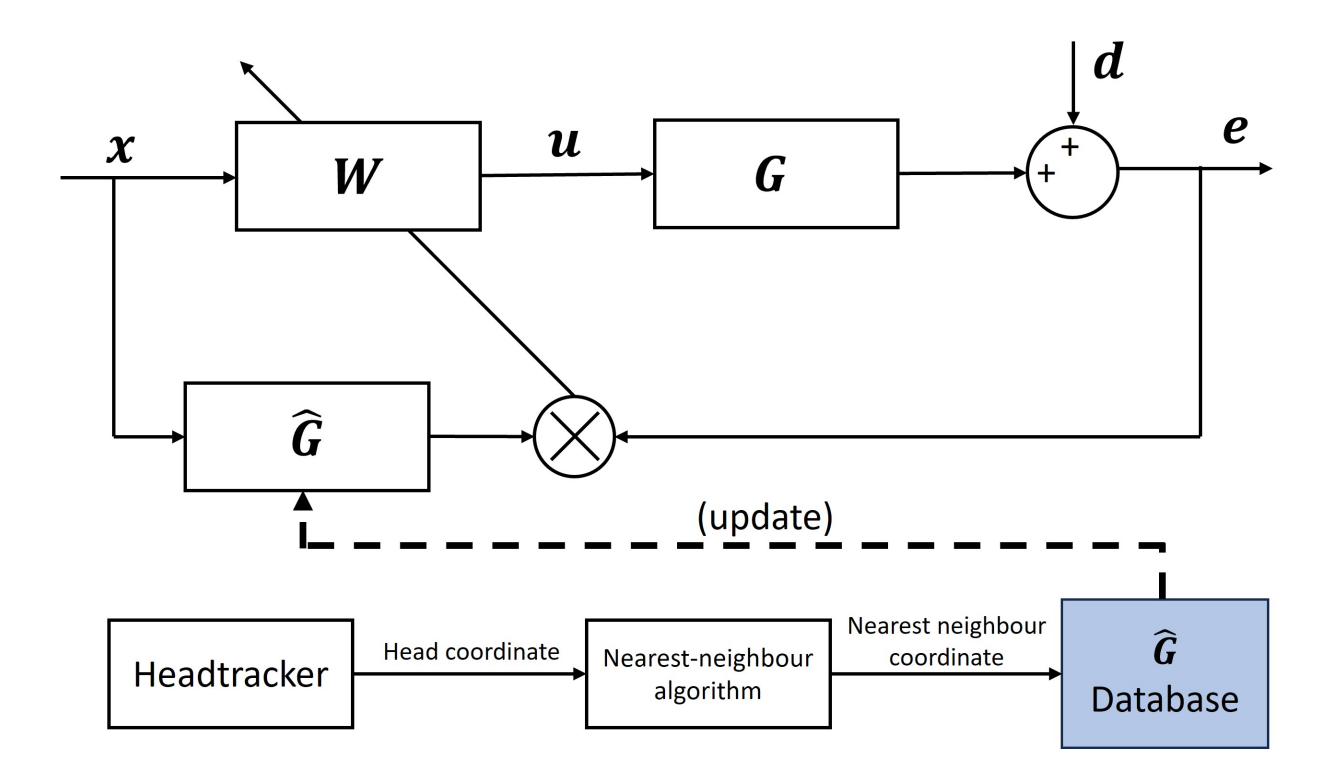


FIG. 3: The multichannel feedforward control system used for the headtracker equipped active headrest system.

In the case where the plant response is approximated by a model, $\hat{\mathbf{G}}$, the vector of control signals can instead be adapted over time to minimise the cost function given by (1) using

the steepest-descent algorithm which is given in this case as

$$\mathbf{u}(n+1) = (1 - \alpha\beta)\mathbf{u}(n) - \alpha\hat{\mathbf{G}}^{\mathrm{H}}\mathbf{e}(n), \tag{4}$$

where α is the step-size which governs the speed of adaptation and the convergence stability and β is the leakage factor that can be tuned to limit the control effort and improve robustness.² Assuming that the controller remains stable throughout its operation, the control signal vector will eventually converge to the steady-state solution, \mathbf{u}_{∞} , given by

$$\mathbf{u}_{\infty} = -\left[\hat{\mathbf{G}}^{\mathrm{H}}\mathbf{G} + \beta\mathbf{I}\right]^{-1}\hat{\mathbf{G}}^{\mathrm{H}}\mathbf{d}.$$
 (5)

In general, this does not converge to the optimal solution given by Equation (3). However, in the case of an active headrest where the system is fully determined (i.e. the number of error signals is equal to the number of control signals), and when the plant response matrices are assumed to be non-singular and where the leakage factor is set to zero, \mathbf{u}_{∞} will be equal to the true optimal value provided by Equation (3). In this case, the steady-state cost function will be equal to the optimum value of zero.²⁶

Since the optimum performance is assured provided the steepest-descent algorithm is stable, it is important to determine the conditions for stability. Through eigenvalue/eigenvector
decomposition²⁷ it can be shown that convergence of the steepest-descent algorithm defined
by Equation (4) is determined by the eigenvalues of the matrix $\hat{\mathbf{G}}^{H}\mathbf{G}$. Specifically, the
convergence condition can be defined in terms of a bound on the step-size given by the
inequality

$$0 < \alpha < \frac{2\operatorname{Re}\left\{\lambda_i + \beta\right\}}{|\lambda_i + \beta|^2} \quad \text{for all } i, \tag{6}$$

where λ_i are the eigenvalues of the $\hat{\mathbf{G}}^{\mathrm{H}}\mathbf{G}$ matrix. This leads to the stability condition that can be expressed as

$$\operatorname{Re}\left\{\operatorname{eig}\left[\hat{\mathbf{G}}^{\mathrm{H}}\mathbf{G} + \beta\mathbf{I}\right]\right\} > 0 \tag{7}$$

where Re $\{\cdot\}$ and eig $[\cdot]$ denote the real and eigenvalue operators, respectively. For the case
where no leakage is introduced, i.e. $\beta = 0$, this stability condition states that all eigenvalues, λ_i , must be positive for the controller to be stable. By introducing a positive leakage factor,
it is possible to force otherwise negative eigenvalues to be positive and thus improve the
robustness of the system to uncertainties in the plant response, with an inherent trade-off
against the steady-state performance. 27,28

$_{ m 212}$ $\,$ III. $\,$ THE EFFECT OF HEAD MOVEMENT ON THE PLANT RESPONSE

This section presents an investigation into the effect of the considered translational and 213 rotational head movements on the plant responses utilising the headrest system plant re-214 sponses measured as described in Section IIA. Figure 4 shows the set of plant responses 215 measured between each loudspeaker and the right ear for all head positions and rotations. 216 In each plot, the thick solid line shows the response measured at the nominal head position 217 with coordinates (0, 0) m and a rotational angle of 0° , whilst the dashed lines show the minimum and maximum bounds for all head positions and rotations. In the case of the direct 219 path, it can be seen from the responses shown in Figure 4a that the magnitude varies by 220 around ± 10 dB, but the shape over frequency is relatively consistent and the level change 221 can thus be largely related to the change in the distance between the loudspeaker and the

ear. From Figure 4c it can be seen that there is also a significant variation in the phase response of the direct path, which can be related to the change in the group delay as the 224 distance between the loudspeaker and the ear varies; this also explains the increasing bounds 225 on the variation in the phase with increasing frequency. It is worth noting that the nominal 226 response at grid position (0, 0) m and 0° rotation is not located at the centre of the grid, 227 as shown in Figure 2, and therefore the corresponding magnitude and phase plots are not 228 centred within the range of responses presented in Figure 4. In the case of the cross-path, 229 shown by the magnitude plot in Figure 4b and the phase plot in Figure 4d, comparable 230 levels of variation in the plant responses with head position and rotation can be observed. 231 However, in the cross-path magnitude response it can be seen that at low frequencies, below around 500 Hz, the level of variation is lower than in the direct-path case, but then gradually 233 increases with frequency before showing very high levels of variation at frequencies above 234 around 1 kHz. This transition in behaviour occurs at frequencies where the head dimen-235 sions become comparable to the acoustic wavelength and several dips can be observed in the 236 cross-path magnitude response due to the nearfield head shadowing effect.²⁹ The frequency 237 where these dips in the magnitude response occur is dependent on the head location and will not be present for all head positions, as shown by the solid line corresponding to the 239 nominal head position and rotation. The influence of the head on the cross-path also widens 240 the bounds in the phase response variation, as shown in Figure 4d, compared to the direct path case. From the responses presented in Figure 4 it is clear that significant levels of plant 242 response variation occur as the head position and rotation vary within the headrest system 243 and this motivates the use of head-tracking to enable the plant response model used in the controller, $\hat{\mathbf{G}}$, to be updated to avoid the need for extremely conservative bounds on the step-size, α , or the inclusion of high levels or leakage, β .

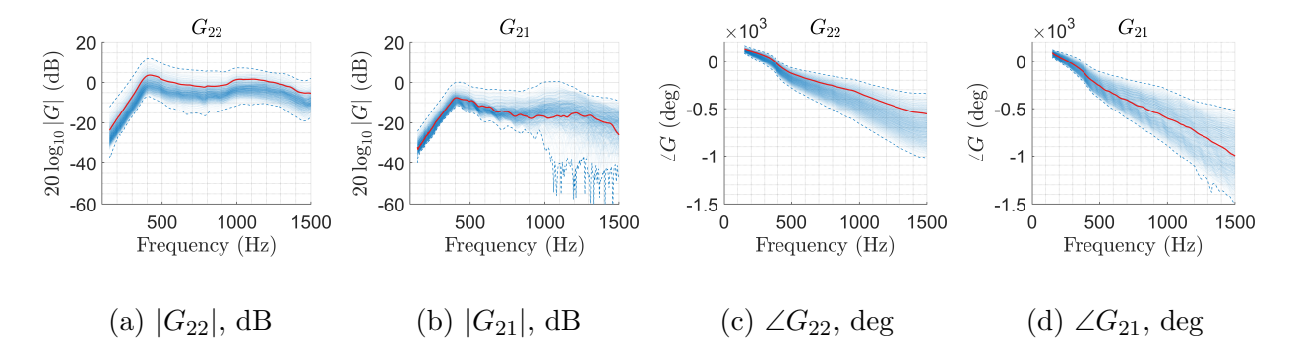


FIG. 4: The plant response between the right and left secondary sources (L2 and L1) and the right error sensor (E2) for all head positions and rotations. The solid lines represent the plant response at the head translational position of (0,0) m with a rotational angle of 0°, and the dashed lines represent the minimum and maximum bounds on the responses for all head positions and rotations described in the schematic diagram presented in Figure 2.

247 248

Although the results presented in Figure 4 show the general effect of head translations 249 and rotations on the plant response, it is useful to explore how rotations alone influence 250 the plant responses. To this end, Figure 5 shows how the magnitude of the plant response 251 varies with head rotation at two different head positions. From Figure 5a it can be seen that 252 for the direct paths $(G_{11} \text{ and } G_{22})$ at the nominal head position head rotation introduces a 253 relatively simple and relatively low level shift in the overall response. However, for the cross 254 paths $(G_{12} \text{ and } G_{21})$ there is a more complicated variation in the responses over frequency 255 as the head shadowing effect varies with angle of rotation. Figure 5b shows similar trends, 256 but due to the translation of the head, the responses are no longer symmetrical and it can be seen that the shift in the magnitude of the response for the G_{22} direct path is much more significant than for the G_{11} direct path. From the results presented in Figure 5 it can be seen that head rotations alone introduce lower levels of plant response variation than when also considering translational head movement, however, it is important to highlight that based on the presented rotational results the effect of rotation does depend on the translational head position.

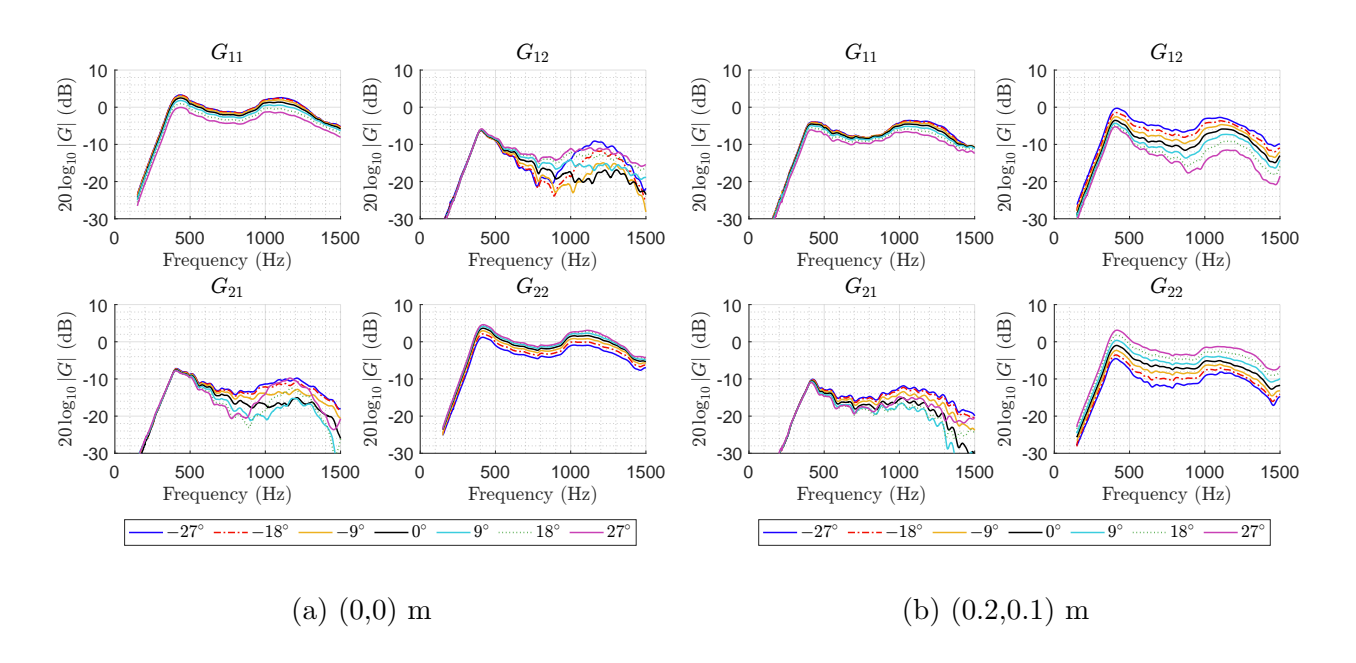


FIG. 5: The magnitude of the plant response between the left and right secondary sources (L1 and L2) and the left and right error sensors (E1 and E2) for all head rotations, at the single head position of (a): (0,0) m and (b): (0.2,0.1) m.

265

264

To consider the effect of head rotations on the phase response of the plant Figure 6 shows
the change in phase due to head rotation relative to the phase response for the 0° head
rotation; this provides further insights into the impact of the head-shadowing effect on the

phase. At the nominal head position, as shown in Figure 6a, it can be seen that there lies an asymmetry in the phase difference between clockwise and anti-clockwise rotations, 270 and the mechanism differs between the direct and cross paths. For the direct paths (G_{11} and G_{22}), since the head shadowing effect in this case is small, the asymmetry in the phase 272 difference between clockwise and anticlockwise rotation is largely due to geometrical acoustic 273 effects between the secondary loudspeakers and the error microphones, which manifest due to changes in the distance between the loudspeaker and the ear. On the other hand, the 275 change in the phase response for the cross-paths $(G_{12} \text{ and } G_{21})$ is caused by nearfield head 276 shadowing effects, which are sensitive to the head orientation relative to the secondary 277 loudspeakers. This behaviour, however, is also dependent on the head position, as shown 278 for the case where the head translational position is (0.2,0.1) m, as presented in Figure 6b. 279 For this head position it is found that the right loudspeaker does not show much asymmetry 280 between the clockwise and anticlockwise rotation for both left and right error microphones. 281 While these detailed changes in the plant responses due to head rotations are physically 282 insightful, because a fully-coupled multichannel control system is considered in this work, 283 their independent direct impact on control stability cannot be easily isolated. That said, 284 the effect of head rotations on the controller stability and performance are investigated in 285 the following section. 286

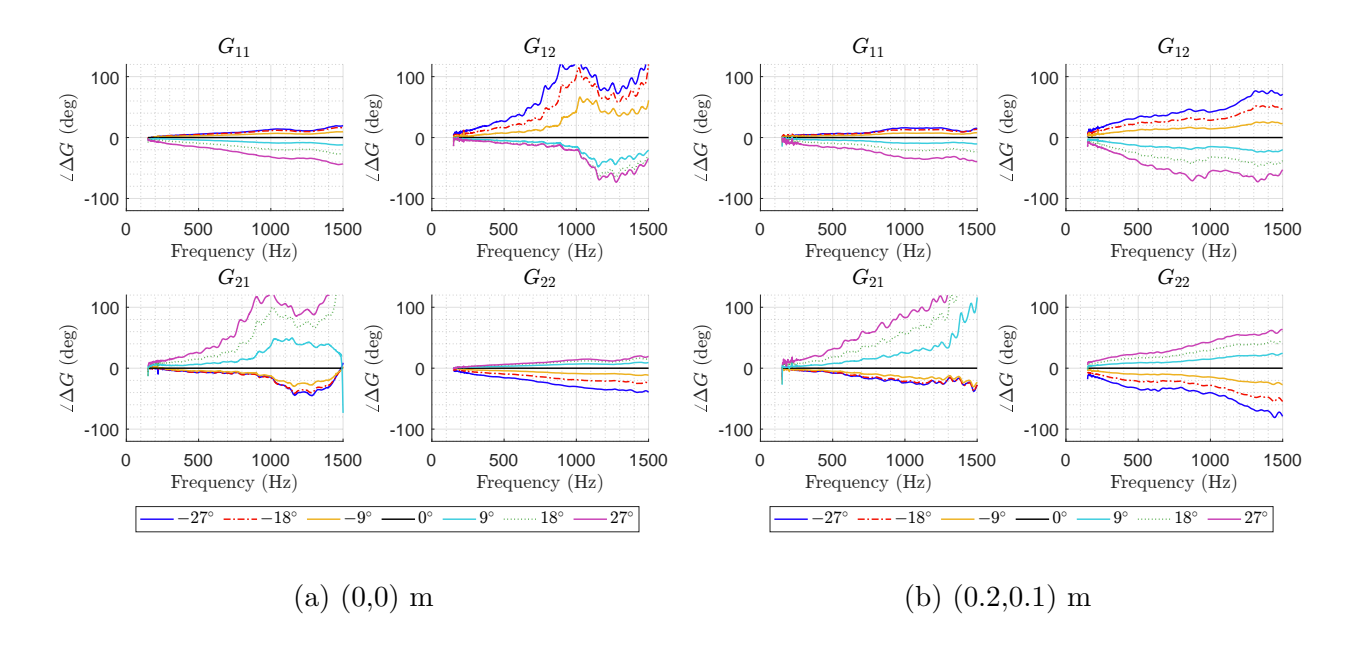


FIG. 6: The difference in the plant response phase relative to the 0° rotational case, in terms of the angle between the left and right secondary sources (L1 and L2) and the left and right error sensors (E1 and E2) for all head rotations, at the single head position of (a): (0,0) m and (b): (0,2,0.1) m.

288 IV. THE EFFECT OF TRACKING RESOLUTION ON CONTROL STABILITY 289 AND CONVERGENCE

The results presented in the previous section have demonstrated how both translational and rotational head movements affect the plant responses in the considered active headrest system. These plant response variations motivate the need to track the head position in order to maximise control performance. Therefore, this section will present a study into how the accuracy of head-tracking, and therefore plant modelling, influences the stability of the feedforward adaptive controller and its convergence behaviour.

A. Effect of tracking resolution on the control stability

296

As shown in Figure 3, the active control system with head-tracking dynamically updates 297 the plant model utilised in the controller, $\hat{\mathbf{G}}$, based on the current position and rotation of 298 the head and a database of plant models. In its most straightforward form, the system will select the plant model from the database that is geometrically closest to the physical head 300 position and rotation determined by the headtracker. Therefore, depending on the resolution 301 of the grid of plant models that forms the database, there will be some error between the physical position of the head and the position to which the plant model corresponds. This 303 geometrical error will in turn lead to an error between the physical plant response, G, 304 and the plant model, G. Figure 7 illustrates the potential geometrical errors between the physical head position/rotation and the modelled head position/rotation, which will lead to 306 errors between the physical plant response G and the plant model \hat{G} . The pink cross/line 307 in each case denotes the modelled head position/rotation, and the coloured arrows denote the physical head positions corresponding to the different levels of position/rotation error. 309 Conceptually, these different levels of error correspond to the use of different grid resolutions 310 in the formation of the plant model database. That is, for translations in the surge and sway directions, the green arrows represent a grid resolution of 2.5 cm, the orange arrows represent 312 a grid resolution of 5 cm, the purple arrows a grid resolution of 7.5 cm, the yellow arrows 313 a grid resolution of 10 cm and the blue arrows a grid resolution of 15 cm; for rotations in 314 yaw, the green arrows represent a grid resolution of 9°, the orange arrows a grid resolution of 18° , the purple arrows a grid resolution of 27° and the yellow arrows a grid resolution of 36° .

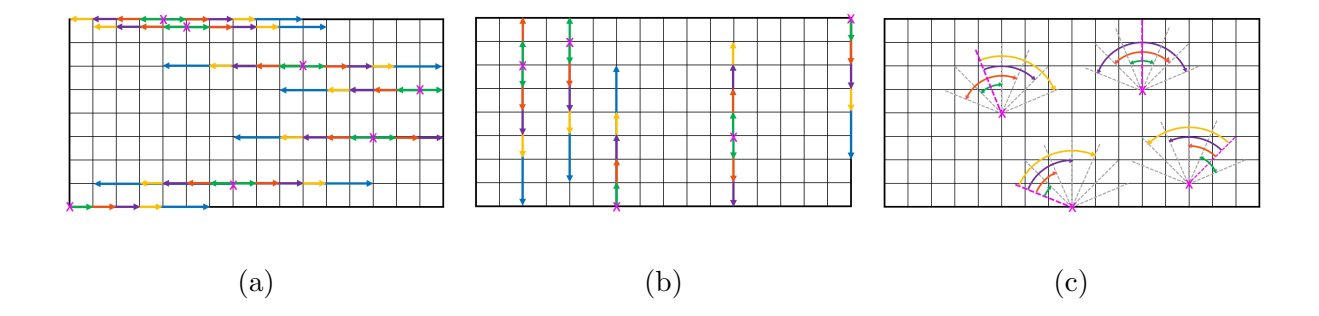


FIG. 7: The potential positioning errors between the physical and modelled head positions in (a) sway (left/right), (b) surge (front/back) and (c) rotational degrees of freedom. The head rotation is assumed to be fixed at 0° for the translational cases.

318 319

The effect of the plant modelling errors due to the tracking resolution on control stability 320 can be assessed via the stability condition given by Equation (7), which states that all 321 eigenvalues of the $\hat{\mathbf{G}}^{\mathrm{H}}\mathbf{G}$ matrix are positive. Figure 8 shows the smallest eigenvalues of $\hat{\mathbf{G}}^{\mathrm{H}}\mathbf{G}$ 322 for the different tracking errors in sway, surge and yaw directions as described in Figure 7 323 for the different grid resolutions. The lines in each of the plots in Figure 8 show the results 324 corresponding to the smallest eigenvalue across all possible tracking errors described by the 325 grids shown in Figure 7, whilst the shaded regions show the range of the smallest eigenvalues 326 for every position on the grid in each case. This means that the lines correspond to the 327 position on the grid where the controller would first go unstable, while the shaded regions 328 give an indication of the range of positions that would be unstable. As perhaps expected, the 329 results in Figure 8 show that the frequency at which an eigenvalue first becomes negative

decreases as the grid resolution decreases, which means that increasing the grid spacing reduces the maximum frequency where the control system remains stable. Focusing on the 332 translational tracking errors in the sway and surge directions, the control instability first occurs at a frequency of 600 Hz and 630 Hz respectively when the lowest resolution grid is 334 utilised, which has a spacing of 0.15 m. As the grid resolution is increased to give a grid 335 spacing of 0.1 m, the frequency at which control instability first occurs increases to 950 Hz and 838 Hz in the sway and surge cases respectively. This increasing trend continues as the 337 grid resolution is further increased up to the reference case shown by the black dashed line, 338 which corresponds to the case where there is no error between the physical and modelled 339 plant positions and so $\hat{\mathbf{G}} = \mathbf{G}$. For the rotational case, even with the lowest tracking 340 resolution assumed here, which corresponds to a 36° spacing, control remains stable at 341 all positions up to around 950 Hz. This can be related to the smaller relative changes in 342 the plant responses observed in Section III for rotational as opposed to translational head 343 movements. However, the trend in stability limits shown in Figure 8 is consistent between the translational and rotational cases, with the frequency at which control instability first 345 occurs increasing as the rotational grid resolution is increased up to the reference case.

In practice, the active noise control headrest should ideally remain stable for all head positions and rotations. It is, however, important to note that the control stability depends on the head position, as represented by the shaded regions in Figure 8. To explore the spatial dependence of the stability limit due to tracking errors, it is insightful to examine the frequencies for which the controller first becomes unstable for each head position. Figure 9 shows the colour plots indicating the frequency at which the control instability first arises

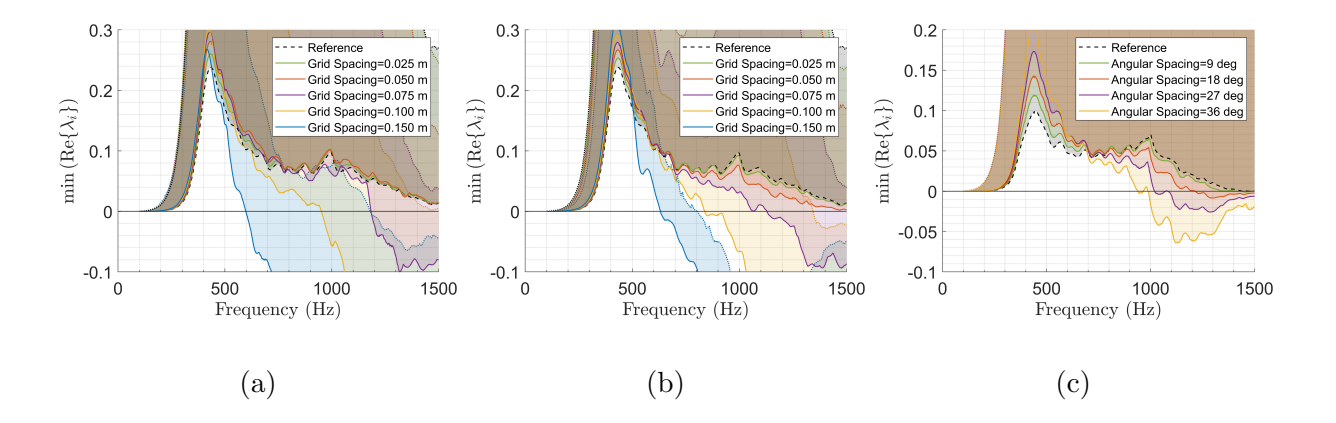


FIG. 8: The set of eigenvalues due to errors in the (a) sway, (b) surge and (c) yaw directions. In the translational cases the head rotation is fixed at 0°. The line plots represent the smallest eigenvalue amongst all possible tracking errors, and the shaded region represents the range of smallest eigenvalues for all considered head movements.

for different tracking resolutions, for each initial head position and the head movements described in Figure 7. For sway movements, as illustrated in Figure 9a, it can be observed 355 that the frequency at which the control system remains stable is the lowest at the head 356 coordinate of $(\pm 0.2, 0)$ m, which corresponds to the line plot in Figure 8a. As the frequency 357 increases, the number of positions where instability occurs increases, and the positions where 358 instability occurs spreads out in the y-direction. For surge movements, as shown in Figure 9b, 359 it can be seen that the frequency at which instability occurs is relatively similar for all head positions, which explains why the shaded region in Figure 8b is relatively narrow. For yaw 361 movements, which are presented in Figure 9c, it can be observed that the frequency at 362 which control instability occurs is the lowest at the head position of $(\pm 0.2, 0.1)$ m, and as frequency increases, the unstable positions spread out towards x=0 m. However, there are still positions where the controller remains stable up to 1500 Hz, as shown by the unfilled region. While the behaviour for the sway and yaw rotation cases are consistent for finer grid resolutions, in the case of surge movements similar trends are not shown for the different tracking resolutions.

As the colour plot in Figure 9 includes head movements in both directions, a spatial 370 discontinuity can be observed, especially for the 0.15 m grid resolution case shown in Fig-371 ure 9a at the $x = \pm 0.05$ m line. To provide further insight into this discontinuity, Figure 10 372 presents the results for sway movement in the positive and negative x-directions separately. 373 Theoretically, the stability condition for head movement between arbitrary positions A and B should be the same as moving the head from position B back to position A, since the 375 real part of the eigenvalue of $\hat{\mathbf{G}}^{\mathrm{H}}\mathbf{G}$ is equal to the real part of the eigenvalue of $\mathbf{G}^{\mathrm{H}}\hat{\mathbf{G}}$. This 376 theoretical stability condition explains the geometrical relationship between the frequency stability limits shown in the colour plots in Figure 10a and Figure 10b. For example, the 378 frequency at which the control system becomes unstable at the initial head position coor-379 dinate (-0.1, 0.125) m when the head sways to the right (Figure 10a) is the same as that at coordinate position (0.05, 0.125) m when the head sways to the left (Figure 10b). For 381 initial head positions in the ranges of $-0.2 \le x \le -0.075$ m and $0.075 \le x \le 0.2$ m, it can 382 be seen that the results presented in the colour plot in Figure 9a are completely governed by the corresponding regions in Figure 10a and Figure 10b for the two regions respectively; 384 this is because movement is only possible in one sway direction within these regions for 385 the assumed configuration. This movement limitation is also indicated by the black regions beyond the x = 0.05 m and x = -0.05 m line for the two plots in Figure 9a. However, for

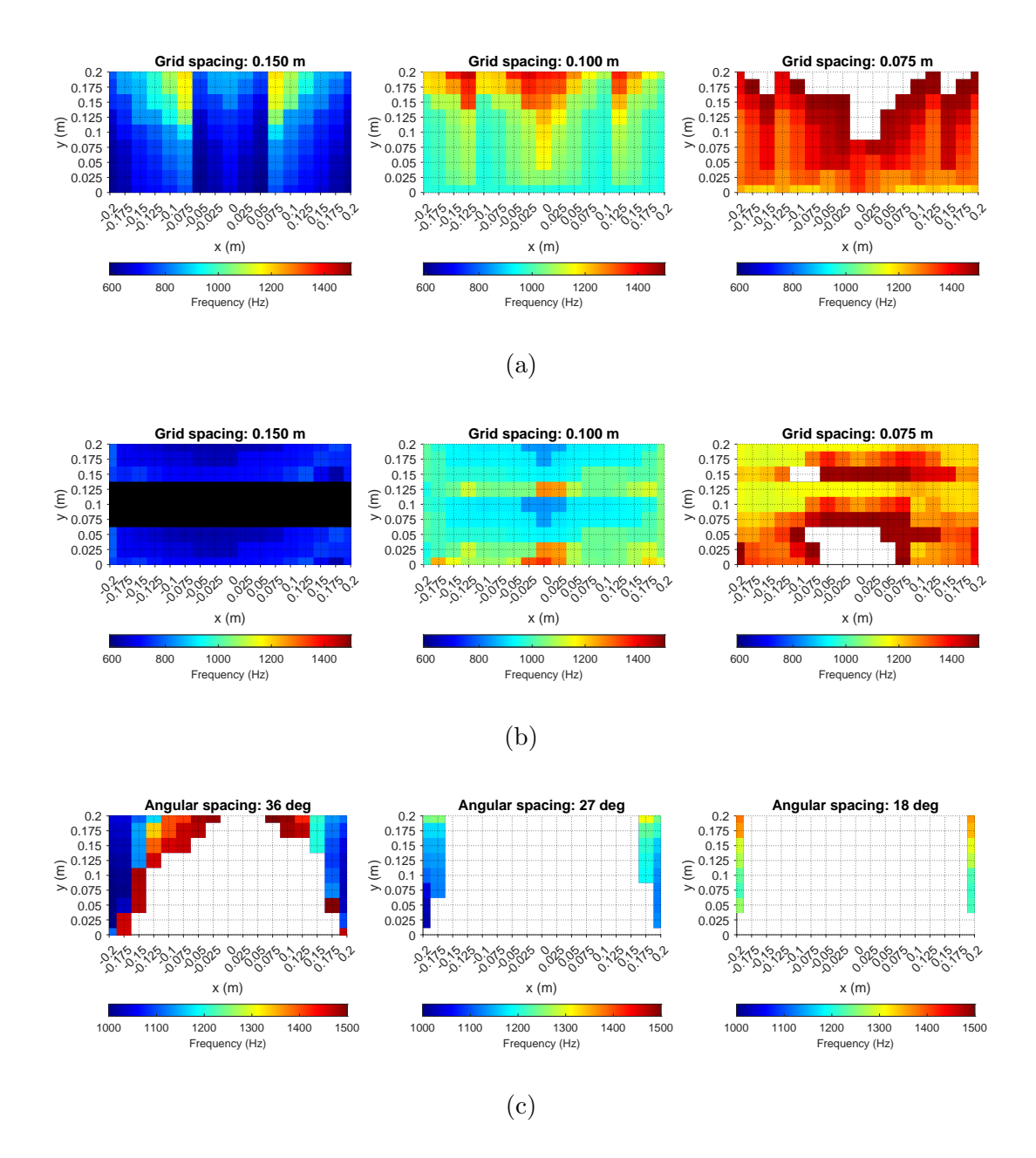


FIG. 9: The colour plots showing the frequency at which instability first occurs for (a): sway (left/right), (b) surge (front/back) and (c): rotation, mapped to the initial head positions within the tracking range. The black regions represent initial head positions where head movement within the specified grid is infeasible, while the unfilled regions denote that the control system at that initial head position remains stable for frequencies up to at least 1500 Hz.

the range of initial head positions $-0.05 \le x \le +0.05$ m, sway movement from an arbitrary initial position A within this range has two possible final head positions, B and C, which 380 represent sway movement in either the positive or negative x-direction. As a result, the colour plot in Figure 9 shows the lowest frequency at which instability arises considering 391 the two possible final head positions, B and C. For example, considering the initial head 392 position (-0.05, 0.125) m, the two possible final head positions are (0.15, 0.125) m in Figure 10a and (-0.2, 0.125) m in Figure 10b. In this case, the two plots in Figure 9a show 394 that the upper frequency limit for control stability is much lower for head movement to the 395 left compared to the case when the head moves to the right. These observations help to explain the discontinuities observed in Figure 9, but also highlight that the frequency at 397 which the control system first becomes unstable depends on the initial head position as well 398 as the direction of head movement.

B. Effect of tracking accuracy on the tonal convergence behaviour

401

Although the results presented in the previous section have demonstrated how the stability of the local ANC system is influenced by the head tracking resolution, this analysis does not consider how the tracking resolution influences the time taken for the system to converge. The speed of convergence is likely to affect the performance of the control system under dynamic conditions, where the head moves over time or where the disturbance signal varies and the controller must adapt to this. This is especially true for frequencies where the eigenvalues are close to 0, assuming the steepest-descent algorithm from Equation (4) is used, since this will result in very slow convergence. The convergence behaviour of the active

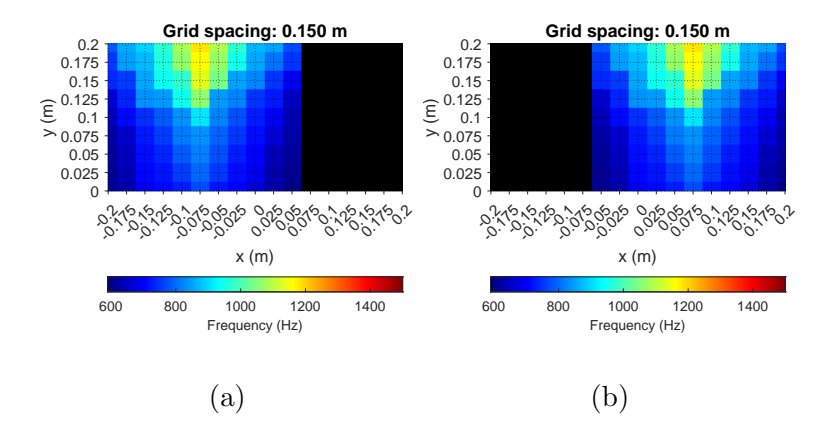


FIG. 10: The colour plots showing, for the grid spacing of 0.15 m, the frequency at which instability first occurs for head sway movement to the (a): right and (b): left, mapped to the initial head positions within the tracking range. The black regions represent the initial head positions where head movement within the specified grid resolution is infeasible.

headrest has been calculated via offline simulations using the measured system responses; previous work has variously demonstrated the consistency between offline simulations and 411 real-time implementation on various digital signal processing platforms.^{2,7,30} Figure 11 il-412 lustrates this behaviour in terms of the average convergence of the error signals for all 413 possible head movements, for different tonal frequencies generated by the primary source. 414 As expected from the stability analysis presented in Section IV A, for the grid resolution of 415 0.15 m for the translational cases the controller diverges for the presented frequencies, since the eigenvalues are negative as previously shown in Figure 8a. For the 0.1 m spacing, on the 417 other hand, the presented convergence results show a slow convergence speed for movement 418 in the sway direction at 900 Hz, which can be linked to the smallest eigenvalue in this case 419 approaching zero.² This is also shown in a similar manner for the case of surge at 900 Hz

and 1010 Hz. While using a 0.1 m grid spacing for 1010 Hz causes the control system to diverge, the 0.075 m grid spacing allows the control system to converge, although the convergence speed is much slower when compared to the case at 800 Hz. For the considered range of rotational movements and resolutions, similar observations are not observed, with the controller only diverging for the largest angular spacing at 1010 Hz. As previously noted in relation to the stability considerations, this smaller difference for the rotational case can be linked back to the smaller effect that rotation has on the plant response, as observed in Figure 5.

430 V. CONCLUSIONS

Incorporating head-tracking techniques into local active noise control headrest systems 431 has previously been shown to enhance control stability and performance when head move-432 ment occurs. While modern head-tracking systems can achieve highly accurate head coordi-433 nate measurements, it is essential in practice to consider the trade-off between the accuracy 434 of the head-tracking system and the complexity of the calibration procedure required to 435 pre-determine the corresponding plant responses. Since the resolution of the calibration procedure needs to be constrained in practice to limit the number of plant responses that 437 need to be measured in advance, the control performance and stability of the headrest system 438 may be affected. This paper has presented an investigation into how the tracking resolution 439 influences the controller limitations in terms of performance and stability.

The results presented in this paper are derived from offline simulations using experimentally measured plant responses for a range of head positions and rotations within a defined

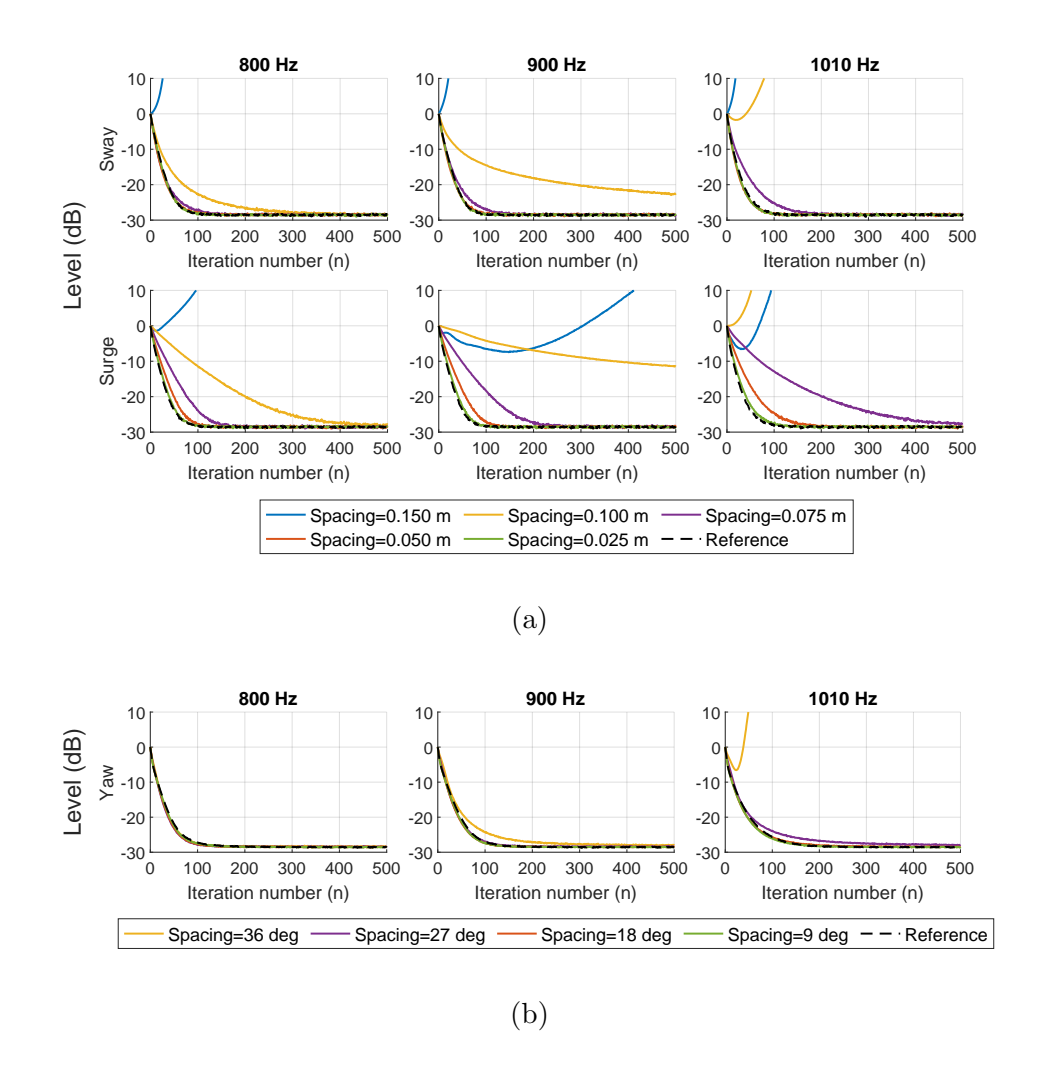


FIG. 11: The convergence of the error signals averaged over all head movements for various tracking resolutions (indicated by the different line-types) and different frequencies (indicated by the plot titles) for (a): sway and surge movements, and (b): yaw rotation. The step size parameter for each head movement is set to a factor of 0.1 times the minimum of $2\text{Re} \{\lambda_i\}/|\lambda_i|^2$.

tracking grid, representing the active headrest noise control system equipped with headtracking. This approach has allowed a systematic study to be conducted to enable a clear insight into the effect of head-tracking accuracy to be provided. The disturbance signals at the ears are assumed to be tonal and known, and they are used directly to realise adaptive control. The effect of varying the resolution of the head-tracking is examined separately across three degrees of freedom: yaw rotation, and translational movements in both the sway and surge directions. Within this context, it has been shown that increasing the tracking resolution generally increases the upper frequency limit at which the control system remains stable, and this frequency depends on the initial position of the head as well as the direction of movement. Although the control system still converges at frequencies approaching this upper frequency limit, due to the small size of the eigenvalues the speed of convergence may be reduced.

The findings presented in this paper can be used to inform the design of an efficient 455 head-tracking calibration procedure. For example, when designing a head-tracked active 456 noise control system, the resolution of head-tracking can be defined based on the highest frequency at which noise control is required. In practice, although the stability limit can 458 be improved for a given tracking grid resolution by introducing leakage into the adaptive 450 control algorithm, this introduces a trade-off between the control stability and the steadystate performance and, therefore, does not enable a coarser tracking grid to be practically 461 employed. It may be possible to utilise interpolation strategies to enable a lower resolution 462 head-tracking grid to be utilised in practice, as suggested elsewhere¹⁵, but further investigation is required. To enable practical realisation in specific applications, it is clearly relevant 464 to consider the impact of reverberant acoustic environments, and to explore how tracking ac-465 curacy for additional degrees of freedom (heave, pitch and roll) influence the control stability and performance.

468 ACKNOWLEDGMENTS

The work was supported by the project IN-NOVA: Active reduction of noise transmitted into and from enclosures through encapsulated structures, which has received funding from the European Union's Horizon Europe programme under the Marie Sklodowska-Curie grant agreement no. 101073037. This work was funded by UK Research and Innovation under the UK government's Horizon Europe funding guarantee [grant number EP/X027767/1]. Jordan Cheer was supported by the Department of Science, Innovation and Technology (DSIT) Royal Academy of Engineering under the Research Chairs and Senior Research Fellowships programme.

477 AUTHOR DECLARATIONS

478 Conflict of Interest

The authors have no conflicts to disclose.

480 DATA AVAILABILITY

The data that support the findings of this study are available from the corresponding author upon reasonable request.

483 REFERENCES

¹P. A. Nelson and S. J. Elliott, *Active control of sound* (Academic Press, 1992).

- ²S. Elliott, Signal Processing for Active Control (Academic Press, 2000).
- ³H. F. Olson and E. G. May, "Electronic Sound Absorber," The Journal of the Acoustical
- Society of America **25**(6), 1130–1136 (1953) doi: 10.1121/1.1907249.
- ⁴B. Rafaely, S. J. Elliott, and J. Garcia-Bonito, "Broadband performance of an active
- headrest," The Journal of the Acoustical Society of America 106(2), 787–793 (1999) doi:
- 490 10.1121/1.427134.
- ⁴⁹¹ ⁵M. Pawelczyk, "Adaptive noise control algorithms for active headrest system," Control
- Engineering Practice **12**(9), 1101–1112 (2004) doi: 10.1016/j.conengprac.2003.11.006.
- ⁶P. Joseph, S. Elliott, and P. Nelson, "Statistical Aspects of Active Control in Harmonic
- Enclosed Sound Fields," Journal of Sound and Vibration 172(5), 629–655 (1994) doi:
- 495 10.1006/jsvi.1994.1203.
- ⁷W. Jung, S. J. Elliott, and J. Cheer, "Combining the remote microphone technique with
- head-tracking for local active sound control," The Journal of the Acoustical Society of
- 498 America **142**(1), 298–307 (2017) doi: 10.1121/1.4994292.
- 8S. J. Elliott, W. Jung, and J. Cheer, "Head tracking extends local active control
- of broadband sound to higher frequencies," Scientific Reports 8(1), 5403 (2018) doi:
- 10.1038/s41598-018-23531-y.
- ⁹C.-Y. Chang, C.-N. Chiou, and S. M. Kuo, "A Complete Design of Smart Pad That
- Reduces Snoring," IEEE Transactions on Consumer Electronics 69(3), 649–656 (2023)
- doi: 10.1109/TCE.2023.3265660.

- ¹⁰L. Yang, L. Zhang, H. Dong, A. Alelaiwi, and A. El Saddik, "Evaluating and Improving
- the Depth Accuracy of Kinect for Windows v2," IEEE Sensors Journal 15(8), 4275–4285
- 507 (2015) doi: 10.1109/JSEN.2015.2416651.
- ⁵⁰⁸ ¹¹C. Lei, J. Xu, J. Wang, C. Zheng, and X. Li, "Active Headrest with Robust Performance
- against Head Movement," Journal of Low Frequency Noise, Vibration and Active Control
- 34(3), 233–250 (2015) doi: 10.1260/0263-0923.34.3.233.
- ¹²H. Chen, X. Huang, H. Zou, and J. Lu, "Research on the Robustness of Active Headrest
- with Virtual Microphones to Human Head Rotation," Applied Sciences 12(22), 11506
- (2022) doi: 10.3390/app122211506.
- ¹³J. Garcia-Bonito, S. J. Elliott, and C. Boucher, "A novel secondary source for a local active
- noise control system," in Active 97, Hungary (1997), pp. 437–450.
- ¹⁴M. Pawelczyk, "Multiple input-multiple output adaptive feedback control strategies for
- the active headrest system: design and real-time implementation," International Journal
- of Adaptive Control and Signal Processing 17(10), 785–800 (2003) doi: 10.1002/acs.778.
- ¹⁵J. Y. Oh, H. W. Jung, M. H. Lee, K. H. Lee, and Y. J. Kang, "Enhancing active noise
- control of road noise using deep neural network to update secondary path estimate in real
- time," Mechanical Systems and Signal Processing **206**, 110940 (2024) doi: 10.1016/j.
- ymssp. 2023.110940.
- ¹⁶J. Buck, S. Jukkert, and D. Sachau, "Performance evaluation of an active headrest con-
- sidering non-stationary broadband disturbances and head movement," The Journal of the
- Acoustical Society of America 143(5), 2571–2579 (2018) doi: 10.1121/1.5034767.

- ¹⁷Z. Yang, Y. Wang, and J. Tao, "Variation of the secondary acoustic paths from loudspeak-
- ers at the seat shoulder in an automobile cabin," in INTER-NOISE and NOISE-CON
- 528 Congress and Conference Proceedings (2023).
- ¹⁸H. Jiang, H. Chen, J. Tao, H. Zou, and X. Qiu, "Accuracy requirements of ear-positioning
- for active control of road noise in a car," Applied Acoustics 225, 110164 (2024) doi:
- 10.1016/j.apacoust.2024.110164.
- ¹⁹S. K. Behera, D. P. Das, and B. Subudhi, "Head movement immune active noise con-
- trol with head mounted moving microphones," The Journal of the Acoustical Society of
- America **142**(2), 573–587 (2017) doi: 10.1121/1.4996125.
- ²⁰T. Xiao, X. Qiu, and B. Halkon, "Ultra-broadband local active noise control with
- remote acoustic sensing," Scientific Reports 10(1), 20784 (2020) doi: 10.1038/
- s41598-020-77614-w.
- ²¹C. K. Lai, J. Cheer, and C. Shi, "The Effect Of Tracking Resolution On The Stability Of
- A Headtracker Equipped Active Headrest Noise Control System," in 30th International
- 540 Congress on Sound & Vibration, International Institute of Acoustics and Vibration (IIAV),
- 541 Amsterdam (2024).
- ²²A. Farina, "Simultaneous Measurement of Impulse Response and Distortion with a Swept-
- Sine Technique," J. Audio Eng. Soc 48, 419–444 (2000).
- ²³H. Li, K. Chen, J. Tao, and X. Qiu, "Using infrared radars for ear positioning in active
- noise control headrests," in INTER-NOISE and NOISE-CON Congress and Conference
- 546 *Proceedings* (2023).

- ²⁴S. Elliott and T. Sutton, "Performance of feedforward and feedback systems for active
- control," IEEE Transactions on Speech and Audio Processing 4(3), 214–223 (1996) doi:
- 10.1109/89.496217.
- ²⁵L. Lu, K.-L. Yin, R. C. De Lamare, Z. Zheng, Y. Yu, X. Yang, and B. Chen, "A survey
- on active noise control in the past decade—Part II: Nonlinear systems," Signal Processing
- 181, 107929 (2021) doi: 10.1016/j.sigpro.2020.107929.
- ²⁶A. Omoto and S. Elliott, "The effect of structured uncertainty in the acoustic plant on
- multichannel feedforward control systems," IEEE Transactions on Speech and Audio Pro-
- cessing **7**(2), 204–212 (1999) doi: 10.1109/89.748125.
- ²⁷S. Elliott, C. Boucher, and P. Nelson, "The behavior of a multiple channel active control
- system," IEEE Transactions on Signal Processing **40**(5), 1041–1052 (1992) doi: 10.1109/
- 78.134467.
- ²⁸S. Elliott and K. Back, "Effort constraints in adaptive feedforward control," IEEE Signal
- Processing Letters **3**(1), 7–9 (1996) doi: 10.1109/97.475821.
- ²⁹D. S. Brungart and W. M. Rabinowitz, "Head-Related Transfer Functions in the Near
- Field:," Defense Technical Information Center, Fort Belvoir, VA (1998), doi: 10.21236/
- 563 ADA399561.
- ³⁰I. Tabatabaei Ardekani and W. Abdulla, "Theoretical convergence analysis of FxLMS
- algorithm," Signal Processing **90**(12), 3046–3055 (2010) doi: 10.1016/j.sigpro.2010.
- 05.009.